

# Search for the Standard Model Higgs Boson in the Lepton + Missing Transverse Energy + Jets Final State in ATLAS

M.S. Neubauer on behalf of the ATLAS Collaboration

Department of Physics, University of Illinois at Urbana-Champaign, Urbana, IL, USA

A search for the Standard Model Higgs boson has been performed in the  $H \rightarrow WW \rightarrow \ell\nu jj$  channel in  $1.04 \text{ fb}^{-1}$  of  $pp$  collisions at  $\sqrt{s} = 7 \text{ TeV}$  collected with the ATLAS detector at the Large Hadron Collider. No significant excess of events is observed over the expected background and limits on the Higgs boson production cross section are derived for a Higgs boson mass in the range  $240 \text{ GeV} < m_H < 600 \text{ GeV}$ . The best sensitivity is reached for  $m_H = 400 \text{ GeV}$ , where the 95% confidence level upper bound on the cross-section for Higgs boson production times the branching ratio for  $H \rightarrow WW$  is  $3.1 \text{ pb}$ , or 2.7 times the Standard Model prediction.

## I. INTRODUCTION

In the Standard Model (SM [1–3]), a scalar field vacuum expectation value breaks the Electroweak symmetry, gives masses to the  $W$  and  $Z$  bosons [4–6], and manifests itself directly as the so-called Higgs boson. A primary goal of the Large Hadron Collider (LHC) is to test the SM mechanism of Electroweak symmetry breaking by searching for Higgs boson production in high energy proton-proton collisions. Thanks in part to the large gluon luminosity at LHC energies [7; 8], the Higgs boson is predominantly produced via gluon fusion ( $gg \rightarrow H$ ) [9–12] and to a lesser extent via weak boson fusion ( $qq \rightarrow qqH$ ) [13–15]. Published limits from direct searches at LEP and the Tevatron exclude  $m_H < 114.4 \text{ GeV}$  [16] and  $162 \text{ GeV} < m_H < 166 \text{ GeV}$  [17] at 95% C.L.

For  $m_H \gtrsim 135 \text{ GeV}$ , the dominant decay mode of the Higgs boson is  $H \rightarrow WW^{(*)}$  [18; 19]. The most sensitive Higgs boson search channel in the range  $135 \lesssim m_H \lesssim 200 \text{ GeV}$  is the purely leptonic mode  $H \rightarrow WW^{(*)} \rightarrow \ell\nu\ell\nu$ . For  $m_H \gtrsim 200 \text{ GeV}$ , the  $H \rightarrow WW \rightarrow \ell\nu jj$  channel, where one  $W$  decays to a pair of jets ( $W \rightarrow jj$ ), also becomes important, along with  $H \rightarrow ZZ$  channels. The advantage of  $H \rightarrow WW \rightarrow \ell\nu jj$  over  $H \rightarrow WW \rightarrow \ell\nu\ell\nu$  for a high mass Higgs boson is the ability to fully reconstruct the Higgs boson mass.

This document describes a search for a Higgs boson in the  $H \rightarrow WW \rightarrow \ell\nu jj$  channel using the ATLAS detector at the LHC, and based on  $1.04 \text{ fb}^{-1}$  of  $pp$  collisions at  $\sqrt{s} = 7 \text{ TeV}$  collected during 2011 [20]. In this analysis, the distribution of the  $\ell\nu jj$  invariant mass  $m(\ell\nu jj)$ , reconstructed using the constraint  $m(\ell\nu) = m(W)$  and the requirement that two of the jets in the event are consistent with a  $W \rightarrow jj$  decay, is used to search for a Higgs boson signal. The results from a previous search for  $H \rightarrow WW \rightarrow \ell\nu jj$  based on  $35 \text{ pb}^{-1}$  of data collected during the 2010 run of LHC were presented in Ref. [21].

The present search, based on the measured shape of the  $m(\ell\nu jj)$  distribution, is restricted to  $m_H > 240 \text{ GeV}$ , in order to ensure a smoothly varying non-resonant background, well clear of the effective kinematic cutoff  $m(\ell\nu jj) \sim 160 \text{ GeV}$ . For  $m_H \gtrsim 600 \text{ GeV}$ , the jets from  $W \rightarrow jj$  decay begin to overlap in the calorimeter, and also the natural width of the Higgs boson becomes large enough that a more detailed treatment of these issues, beyond the scope of the present analysis, might be required. The best sensitivity in this analysis occurs for  $m_H \sim 400 \text{ GeV}$ .

## II. DETECTOR

The ATLAS detector [22] is a multipurpose particle physics apparatus with forward-backward symmetric cylindrical geometry covering  $|\eta| < 2.5$  for tracks and  $|\eta| < 4.9$  for jets [41]. The inner tracking detector (ID) consists of a silicon pixel detector, a silicon microstrip detector, and a transition radiation tracker. The ID is surrounded by a thin superconducting solenoid providing a 2 T magnetic field, and by a high-granularity liquid-argon (LAr) sampling electromagnetic (EM) calorimeter. An iron-scintillator tile calorimeter provides hadronic coverage in the central rapidity range. The end-cap and forward regions are instrumented with LAr calorimetry for both electromagnetic and hadronic measurements. The muon spectrometer surrounds the calorimeters and consists of three large superconducting toroids, each with eight coils, a system of precision tracking chambers, and detectors for triggering.

Detailed Monte Carlo (MC) studies of signal and backgrounds have been carried out. The interaction with the ATLAS detector is modeled using GEANT4 [23] and the events are reconstructed using the same software that is used to perform the reconstruction on data. The effect of multiple  $pp$  interactions occurring at high luminosities (pile-up) is simulated in the MC samples by superimposing at the generation stage several simulated minimum-bias events on the simulated signal and background events. MC samples corresponding to several different sets of pile-up conditions were generated and subsequently re-weighted to match the observed pile-up conditions for the present data set.

### III. DATASET AND TRIGGER

The data used in this analysis were recorded during periods when stable beams were present, and all ATLAS sub-detectors were operating under nominal conditions. The events were triggered by requiring the presence of an electron candidate with transverse energy  $E_T > 20$  GeV or a muon candidate with transverse momentum  $p_T > 18$  GeV.

### IV. OBJECT SELECTION

Electron candidates are selected from clustered energy deposits in the EM calorimeter with an associated track and are required to satisfy a tight set of identification cuts [24] with an efficiency of  $71 \pm 1.6\%$  for electrons with  $E_T > 20$  GeV. While the energy measurement is taken from the EM calorimeter, the pseudorapidity  $\eta$  and azimuthal angle  $\phi$  are taken from the associated track. The cluster is required to be in  $|\eta| < 2.47$ , outside  $1.37 < |\eta| < 1.52$ , and in a region where the calorimeter was known to be operating normally at the time the event was recorded. The track associated with the electron candidate is required to point back to a reconstructed primary vertex with a transverse impact parameter significance  $\leq 10\sigma$  and an impact parameter along the beam direction  $\leq 10$  mm. Electrons are required to be isolated: the sum of the transverse energies of cells inside a cone  $\Delta R < 0.3$  [42] around the cluster centroid (excluding the electron itself) must satisfy  $\Sigma(E_T^{calo}) < 4$  GeV.

Muons are reconstructed by combining tracks in the inner detector and muon spectrometer [25]. The efficiency of this reconstruction is  $92 \pm 0.6\%$  for muons with  $p_T > 20$  GeV. Muons are required to satisfy basic quality cuts on the number and type of hits in the inner detector. They must lie in  $|\eta| < 2.4$ , satisfy the same impact parameter cuts as electrons, and be isolated, with the sum of track transverse momenta in a cone  $\Delta R < 0.2$  around the muon satisfying  $\Sigma(p_T^{track})/p_T^\mu < 0.1$ .

Jets are reconstructed from calibrated topological clusters using the anti- $k_t$  algorithm [26] with radius parameter  $R = 0.4$ . The reconstructed jets are calibrated using an  $E_T$  and  $\eta$  dependent correction factor based on MC simulation. They are required to have  $E_T > 25$  GeV and  $|\eta| < 4.5$ . Jets are  $b$ -tagged if they contain a reconstructed displaced secondary vertex consistent with a  $b$ -decay. The missing transverse energy  $\cancel{E}_T$  in the event is reconstructed starting from topological energy clusters in the calorimeters calibrated according to the type of the object to which they belong and accounting also for muons, since muons generally deposit little of their energy in the calorimeters.

### V. EVENT SELECTION

The primary vertex in selected events is required to consist of  $\geq 3$  tracks with  $p_T > 400$  MeV. There must be exactly one reconstructed lepton candidate (electron or muon) with  $p_T > 30$  GeV. In order to ensure that this analysis is statistically independent of the ATLAS  $H \rightarrow ZZ \rightarrow \ell\ell\nu\nu$  analysis and thus allow the computation of combined limits in a future study, events are vetoed if there is any additional lepton with  $p_T > 20$  GeV, including electrons which only satisfy the looser identification cuts used in the  $H \rightarrow ZZ \rightarrow \ell\ell\nu\nu$  analysis [27].

Events are required to have  $\cancel{E}_T > 30$  GeV consistent with an unobserved neutrino from  $W \rightarrow \ell\nu$  decay. There must be exactly two jets ( $H + 0$  jet sample) or exactly three jets ( $H + 1$  jet sample) having  $E_T > 25$  GeV and  $|\eta| < 4.5$ . The two jets with invariant mass closest to the mass of the  $W$  boson are required to satisfy  $71 \text{ GeV} < m_{jj} < 91 \text{ GeV}$ . These two jets are taken as the  $W$  decay jets and are required to lie in the range  $|\eta| < 2.8$ , where the jet energy scale (JES) is known to better than  $\pm(4-8)\%$  for  $E_T > 25$  GeV.

The mass constraint equation  $m(\ell\nu) = m(W)$  is used to reconstruct  $m(\ell\nu jj)$  (taking  $p_T^\nu$  from  $\cancel{E}_T$ ) and can have real or complex solutions. In the case of a complex solution, the event is rejected, while in the case of two real solutions, the solution with smaller  $|p_z^\nu|$  is taken, based on studies using simulation.

After the event selection, the background is expected to be dominated by  $W$ +jets production. Other important backgrounds are  $Z$ +jets, multijets (MJ) from QCD processes, top quark and diboson ( $WW$ ,  $WZ$ , and  $ZZ$ ) production. In order to further reject backgrounds from top quark production, events are rejected if any of the jets passes the  $b$ -tagging criteria. The efficiency and mistag rate of the  $b$ -tagging have been measured using the methods described in Ref. [28] and are well modeled in the MC simulation.

## VI. SIGNAL AND BACKGROUND MODELING

Although MC is not used to model the background in the final fit used to obtain limits, a combination of MC and data-driven models are used to better understand the background yields at this intermediate stage. Both the gluon fusion and the weak boson fusion signal production processes are modeled at NLO using the POWHEG + PYTHIA event generators [29–31]. Table I shows the cross-sections for the gluon fusion and weak boson fusion signal processes in the SM [19].

Backgrounds due to  $W/Z$ +jets,  $t\bar{t}$ , and diboson production are modeled using the ALPGEN [32], MC@NLO [33], and HERWIG [34] generators, respectively. A small contribution from  $W/Z + \gamma$  events is modeled using MadEvent [35]. The MJ background is modeled using templates derived from the data selected in an identical way to the  $H \rightarrow WW \rightarrow \ell\nu jj$  selection except that the electron identification requirements are loosened (electrons satisfying the complete set of identification criteria are vetoed) and the isolation requirement on muons is inverted. Expected contributions from non-QCD processes to the MJ templates are subtracted using absolute MC predictions. The normalizations for the MJ and  $W/Z$ +jets contributions are determined by a fit at this stage to the  $\cancel{E}_T$  distribution with all cuts applied except for the  $\cancel{E}_T > 30$  GeV requirement and with the sum of top and diboson backgrounds fixed to its expectation in  $1.04 \text{ fb}^{-1}$  of integrated luminosity.

TABLE I: Cross-sections for Higgs boson production and the branching ratio for  $H \rightarrow WW \rightarrow \ell\nu jj$  ( $\ell = e/\mu$ ) in the Standard Model.

$m_H$ [GeV]	$\sigma(gg \rightarrow H)$ [pb]	$\sigma(qq \rightarrow H)$ [pb]	$\text{BR}(H \rightarrow \ell^\pm \nu jj)$
300	$2.4 \pm 0.4$	$0.30^{+0.014}_{-0.008}$	0.202
400	$2.0^{+0.31}_{-0.34}$	$0.162^{+0.010}_{-0.005}$	0.170
500	$0.85 \pm 0.15$	$0.095^{+0.0068}_{-0.0032}$	0.160
600	$0.33^{+0.063}_{-0.058}$	$0.058^{+0.005}_{-0.002}$	0.164

## VII. RESULTS

Table II shows the observed and expected yields for signal and background, after the full event selection except for the requirement that  $m(\ell\nu) = m(W)$  has a real solution, for each jet multiplicity and flavor category and for their sum.

Figure 1 (top) shows the  $m(\ell\nu jj)$  distribution, including the requirement that  $m(\ell\nu) = m(W)$  has a real solution, summed over all lepton flavors and jet multiplicities. The SM signal with  $m_H = 400$  GeV is also shown, scaled up by a factor of 2.7.

Limits are set using a maximum likelihood fit to the shape of the observed  $m(\ell\nu jj)$  distribution in the range  $200 < m(\ell\nu jj) < 2000$  GeV. The non-resonant background in this fit is modeled by the sum of two exponential functions. The normalization and slope of each exponential are free parameters in the fit. The double-exponential form for the total background is well justified by fits to the  $m(\ell\nu jj)$  distributions obtained by selecting events with  $m_{jj}$  just below ( $50 < m_{jj} < 60$  GeV) or just above ( $100 < m_{jj} < 110$  GeV) the  $W$  peak, respectively. The  $m(\ell\nu jj)$  distribution for the signal at each hypothesized  $m_H$  is modeled using the signal MC samples.

TABLE II: Observed and expected event yields in  $1.04 \text{ fb}^{-1}$  of data, for SM Higgs boson production and significant backgrounds after all cuts for the  $H + 0j$  and  $H + 1j$  search channels, prior to the requirement that  $m(\ell\nu) = m(W)$  has a real solution. For the  $W/Z$ +jets and MJ backgrounds, the uncertainties are taken from a fit to the  $\cancel{E}_T$  distribution which normalizes these backgrounds and the total error in the rightmost column is the sum in quadrature since the fit errors are statistically independent. For signal, top and diboson production, the quoted uncertainties are JES ( $\pm 17\%$ ), cross-section ( $\pm 10\%$  for both top and diboson), and luminosity ( $\pm 3.7\%$ ) and are added in quadrature; the total errors in the rightmost column for these contributions are the linear sum of the errors for the individual channels since these sources of systematic uncertainty are correlated across channels. Statistical errors are small here compared to these uncertainties.

	$H(\ell\nu jj) + 0j$	$H(\mu\nu jj) + 0j$	$H(\ell\nu jj) + 1j$	$H(\mu\nu jj) + 1j$	$H + 0j \text{ or } 1j$
$W/Z$ +jets	$10780 \pm 290$	$13380 \pm 870$	$6510 \pm 250$	$7410 \pm 670$	$38080 \pm 1160$
Multi-jet	$890 \pm 24$	$256 \pm 17$	$669 \pm 25$	$212 \pm 19$	$2027 \pm 43$
Top	$170 \pm 34$	$164 \pm 33$	$489 \pm 98$	$500 \pm 100$	$1320 \pm 270$
Dibosons	$397 \pm 79$	$414 \pm 83$	$161 \pm 32$	$204 \pm 41$	$1180 \pm 240$
Expected Background	$12240 \pm 300$	$14210 \pm 870$	$7830 \pm 270$	$8330 \pm 680$	$42600 \pm 1200$
Observed	11988	13906	7543	8250	41687
Expected Signal ( $m_H = 400 \text{ GeV}$ )	$14 \pm 3.6$	$12 \pm 3.1$	$18 \pm 4.7$	$14 \pm 3.6$	$58 \pm 15$

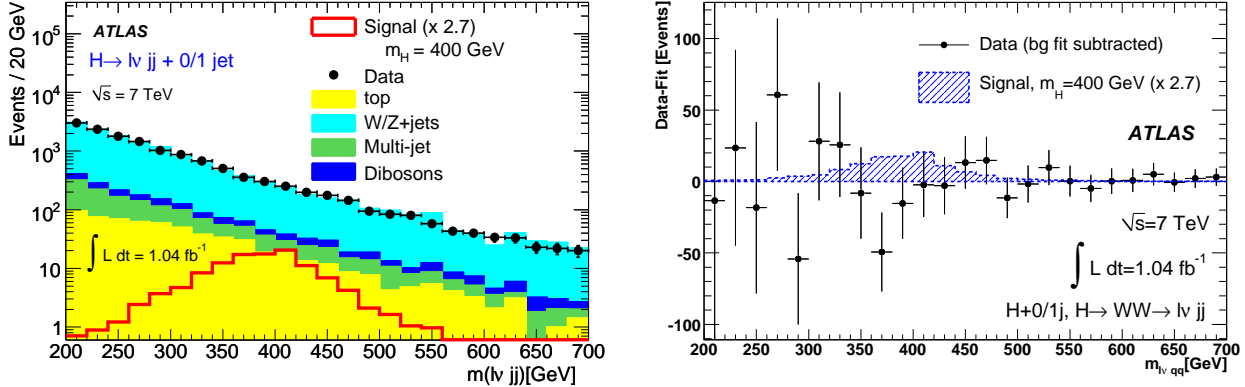


FIG. 1: The distribution of the invariant mass  $m(\ell\nu jj)$ , summed over lepton flavor and jet multiplicity. Top: the comparison between data and MC. Bottom: the difference between data and the fitted non-resonant background. The expected contribution from Higgs boson decays for  $m_H = 400 \text{ GeV}$  in the SM is also shown, multiplied by a factor of 2.7.

The fit accounts for the uncertainty in the efficiency of the electron, muon, and jet reconstruction. The electron and muon efficiencies are varied within their uncertainties, leading to an uncertainty in the signal efficiency of  $\pm 1.6\%$  and  $\pm 0.6\%$ , for electrons and muons respectively. Varying the jet energy scale within its uncertainties yields a corresponding uncertainty of  $\pm 17\%$ , and smearing the jet energies within the uncertainty on their resolutions results in an uncertainty of  $\pm 8.6\%$ . The limits also take into account a  $\pm 3.7\%$  uncertainty on the luminosity determination and a  $\pm 19.4\%$  uncertainty on the predicted signal cross-section [19], taken to be independent of mass.

Effects due to the finite width of the Higgs boson and due to interference between Higgs boson and SM processes, which were discussed in Refs. [19; 36], have been neglected. If an additional uncertainty of  $150 \times m_H^3\%$  (where  $m_H$  is in TeV) were to be assigned for this, it would increase the total systematic error by  $< 6\%$  for  $m_H \leq 500 \text{ GeV}$ , but as much as  $15\%$  for  $m_H = 600 \text{ GeV}$  where the impact on the limit is about  $18\%$ .

Figure 1 (right) shows the difference between the  $m(\ell\nu jj)$  distribution in data and the fitted background. There is no indication of any significant excess, so limits are extracted using the Profile Likelihood [37] as a test statistic and following the  $CL_s$  procedure described in Ref. [38]. Figure 2 shows the 95% CL upper

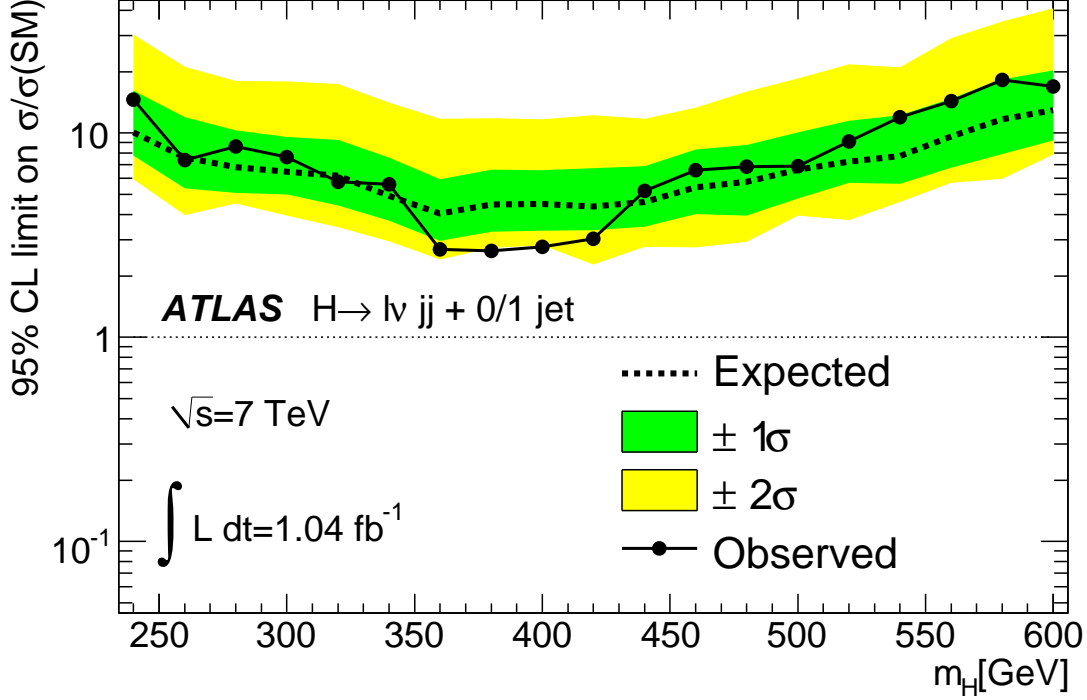


FIG. 2: The expected and observed 95% confidence level upper limits on the Higgs boson production cross-section ratio with the SM cross-section in  $1.04 \text{ fb}^{-1}$  of data. For any hypothesized Higgs boson mass, the background contribution used in the calculation of this limit is set by the background distribution obtained from the fit to the  $m(\ell\nu jj)$  distribution.

bound on  $\sigma \times BR_{H \rightarrow WW} / (\sigma \times BR_{H \rightarrow WW})_{\text{SM}}$  as a function of  $m_H$ . The 95% confidence level in the data for  $m_H = 400 \text{ GeV}$  is 3.1 pb, or 2.7 times the SM prediction. In the Standard model with an additional heavy fourth generation (SM4) [39; 40] the gluon fusion mechanism for production of a Higgs boson is expected to be substantially enhanced. Within the SM4 context, a Higgs boson is excluded at 95% CL by the present data over the range  $m_H = 310 - 430 \text{ GeV}$ .

- 
- [1] S. Weinberg, Phys. Rev. Lett. **19**, 1264 (1967).
  - [2] S. L. Glashow, Nucl. Phys. **B22**, 579 (1961).
  - [3] A. Salam, in *Elementary Particle Theory*, p. 367 (Almqvist and Wiksell, Stockholm, 1968).
  - [4] F. Englert and R. Brout, Phys. Rev. Lett. **13**, 321 (1964).
  - [5] P. W. Higgs, Phys. Lett. **12**, 132 (1964).
  - [6] G. S. Guralnik, C.R. Hagen and T.W.B. Kibble, Phys. Rev. Lett. **13**, 585 (1964).
  - [7] H.-L. Lai, M. Guzzi, J. Huston, Z. Li, P. M. Nadolsky, et al., Phys.Rev. **D82**, 074024 (2010).
  - [8] A. Sherstnev and R. S. Thorne, Eur. Phys. J. **C55**, 553 (2008).
  - [9] C. Anastasiou, R. Boughezal, and F. Petriello, JHEP **04**, 003 (2009).
  - [10] D. de Florian and M. Grazzini, Phys. Lett. **B674**, 291 (2009).
  - [11] U. Aglietti, R. Bonciani, G. Degrassi, and A. Vicini, Phys. Lett. **B595**, 432 (2004).
  - [12] S. Actis, G. Passarino, C. Sturm, and S. Uccirati, Phys. Lett. **B670**, 12 (2008).
  - [13] P. Bolzoni, F. Maltoni, S.-O. Moch, and M. Zaro, Phys. Rev. Lett. **105**, 011801 (2010), 1003.4451.
  - [14] M. Ciccolini, A. Denner, and S. Dittmaier, Phys. Rev. Lett. **99**, 161803 (2007), 0707.0381.

- [15] M. Ciccolini, A. Denner, and S. Dittmaier, Phys. Rev. **D77**, 013002 (2008), 0710.4749.
- [16] The LEP Collaborations, Phys. Lett. **B565**, 61 (2003).
- [17] T. Aaltonen et al. (CDF Collaboration), Phys. Rev. Lett. **104**, 061802 (2010).
- [18] A. Bredenstein, A. Denner, S. Dittmaier, and M. M. Weber, JHEP **0702**, 080 (2007).
- [19] LHC Higgs Cross Section Working Group, S. Dittmaier, C. Mariotti, G. Passarino, and R. Tanaka (Eds.), CERN-2011-002 (CERN, Geneva, 2011), arXiv:1101.0593.
- [20] The ATLAS Collaboration (2011), arXiv:1109.3615, submitted to *Phys. Rev. Lett.*
- [21] The ATLAS Collaboration (2011), arXiv:1106.2748, submitted to EPJC.
- [22] The ATLAS Collaboration, JINST **3**, S08003 (2008).
- [23] S. Agostinelli et al., NIM A **506**, 250 (2003).
- [24] The ATLAS Collaboration, JHEP **12**, 060 (2010).
- [25] The ATLAS Collaboration, JHEP **2010**, 1 (2010).
- [26] M. Cacciari, G. P. Salam, and G. Soyez, JHEP **04**, 063 (2008).
- [27] The ATLAS Collaboration, ATLAS Conference Note ATLAS-CONF-2011-026, available online at <http://cdsweb.cern.ch/record/1336759> (2011).
- [28] The ATLAS Collaboration, ATLAS Conference Note ATLAS-CONF-2011-089, available online at <http://cdsweb.cern.ch/record/1356198> (2011).
- [29] T. Sjöstrand et al., JHEP **05**, 026 (2006).
- [30] S. Alioli et al., JHEP **04**, 002 (2009).
- [31] P. Nason and C. Oleari, JHEP **02**, 037 (2010), 0911.5299.
- [32] M. L. Mangano et al., JHEP **07**, 001 (2003).
- [33] S. Frixione and B. Webber, JHEP **0308**, 007 (2003).
- [34] G. Corcella et al., JHEP **01**, 010 (2001).
- [35] J. Alwall et al., JHEP **09**, 028 (2007).
- [36] C. Anastasiou, S. Buehler, F. Herzog, and A. Lazopoulos (2011), arXiv:1107.0683.
- [37] G. Cowan et al., Eur. Phys. J. **C71**, 1554 (2011).
- [38] A. L. Read, *Modified frequentist analysis of search results (the  $CL_s$  method)*, CERN-OPEN-2000-205, available online at <http://cdsweb.cern.ch/record/451614> (2000).
- [39] G. D. Kribs, T. Plehn, M. Spannowsky, and T. M. Tait, Phys.Rev. **D76**, 075016 (2007), 0706.3718.
- [40] Becerici Schmidt, N., Çetin, S. A., İstin, S., and Sultansoy, S., Eur. Phys. J. C **66**, 119 (2010).
- [41] ATLAS uses a right-handed coordinate system with its origin at the nominal interaction point (IP) in the center of the detector and the  $z$ -axis coinciding with the axis of the beam pipe. The  $x$ -axis points from the IP to the center of the LHC ring, and the  $y$ -axis points upward. Cylindrical coordinates  $(r, \phi)$  are used in the transverse plane,  $\phi$  being the azimuthal angle around the beam pipe. The pseudorapidity is defined in terms of the polar angle  $\theta$  as  $\eta = -\ln \tan(\theta/2)$ .
- [42]  $\Delta R = \sqrt{\Delta\phi^2 + \Delta\eta^2}$ .